J. Mol. Biol. (1997) **274**, 72–83

JMB

Structure and Dynamics of the Iron Responsive Element RNA: Implications for Binding of the RNA by Iron Regulatory Binding Proteins

Kenneth J. Addess[1], James P. Basilion[2], Richard D. Klausner[2] Tracey A. Rouault[2] and Arthur Pardi[1]*

[1]*Department of Chemistry and Biochemistry, University of Colorado, Boulder CO 80309-0215, USA*

[2]*Cell Biology and Metabolism Branch, National Institute of Child Health Development National Institutes of Health Bethesda, MD 20892, USA*

**Corresponding author*

The iron responsive element (IRE) is a ~30 nucleotide RNA hairpin that is located in the 5′ untranslated region of all ferritin mRNAs and in the 3′ untranslated region of all transferrin receptor mRNAs. The IREs are bound by two related IRE-binding proteins (IRPs) which help control intracellular levels of iron by regulating the expression of both ferritin and transferrin receptor genes. Multi-dimensional NMR and computational approaches were used to study the structure and dynamics of the IRE RNA in solution. The NMR data are consistent with formation of *A*-form helical stem regions, a one-base internal bulge and a Watson-Crick C·G base-pair between the first and fifth nucleotides in the loop. A superposition of refined structures indicates that the conserved C in the internal bulge, and three residues in the six-nucleotide hairpin loop are quite dynamic in this RNA. The structural roles of the stems, the loop and the bulge in the function of the IRE RNA and in possible interactions with the iron regulatory protein are discussed.

Keywords: iron regulation; RNA structure; hairpin loops and bulges; IRP; NMR structure

Introduction

Iron homeostasis is maintained in mammalian cells through post-transcriptional regulation of genes coding for ferritin, a protein that sequesters iron from the cytoplasm of eukaryotic cells, and the transferrin receptor (TfR), a protein that delivers iron to the cytoplasm by receptor-mediated endocytosis (Klausner *et al.*, 1993; Hentze & Kuhn, 1996). A *cis*-acting component of post-transcriptional regulation of both genes is a 30-nucleotide hairpin loop RNA known as the iron responsive element (IRE; Aziz & Munro, 1987; Hentze *et al.*, 1987). IREs are located within the 5′ untranslated region of all ferritin mRNAs and the 3′ untranslated region of all transferrin receptor mRNAs. They are bound with high affinity by two related IRE binding proteins now known as iron regulatory protein 1 (IRP1) and iron regulatory protein 2 (IRP2; Rouault *et al.*, 1992; Samaniego *et al.*, 1994; Guo *et al.*, 1994). IRP1 is a bifunctional cytosolic protein with its function determined by the presence or absence of a [4Fe-4S] cluster. When a eukaryotic cell is depleted of iron, the iron-free form of IRP1 binds with high affinity to the IRE. When bound to the RNA, the protein represses the expression of ferritin by preventing the binding of translational initiation factors to the 5′ cap site of the ferritin mRNA (Gray & Hentze, 1994). It simultaneously increases the expression of the TfR gene by protecting the TfR mRNA against degradation by cellular ribonucleases (Binder *et al.*, 1994).

Phylogenetic comparison and sequence analysis of naturally occurring IREs were used to define a

Present addresses: K. J. Addess, Computational Biology Branch, National Center for Biotechnology Information, National Library of Medicine, National Institutes of Health, Bethesda, MD 20894, USA; J. P. Basilion, Variagenics, Inc., 1 Kendall Square, Building 400, Cambridge, MA 02139, USA.

Abbreviations used: IRE, iron responsive element; NTP, nucleotide 5′-triphosphate; IRP, iron regulatory protein; TfR, transferrin receptor; mRNA, messenger RNA; DEAE, diethylaminoethyl; NOE, nuclear Overhauser effect; NOESY, nuclear Overhauser effect spectroscopy; COSY, correlation spectroscopy; TOCSY, total correlation spectroscopy; E.COSY, exclusive correlation spectroscopy; HSQC, heteronuclear single quantum coherence; CT-HSQC, constant time heteronuclear single quantum coherence; CPMG, Carr-Purcell-Meiboom-Gill sequence; RMSD, root-mean-square deviation.

0022–2836/97/460072–12 $25.00/0/mb971377

28-nucleotide minimal consensus sequence of the RNA, which consists of two stem regions separated by a single bulged cytosine located five base-pairs away from a six-nucleotide loop (Barton *et al*., 1990; Bettany *et al*., 1992; Jaffrey *et al*., 1993; Theil, 1994). All known IREs contain a highly conserved six-base loop of the sequence 5′-CAGUGX-3′, where X at position 6 can be either an A, C or U but never a G. The stem regions of the IRE must form stable double helices but there is generally no sequence requirement for high-affinity binding by IRP1. The lower stem varies in the number of complementary base-pairs whereas there is a strict requirement for five base-pairs in the upper stem for RNA function (Kikinis *et al*., 1995; Jaffrey *et al*., 1993). Chemical protection experiments and mutational analysis of the consensus sequence indicate that the fold of the IRE conforms to its predicted secondary structure (Bettany *et al*., 1992; Harrell *et al*., 1991; Wang *et al*., 1991, 1990).

Competition studies of the consensus IRE with RNAs containing single mutations in the loop or bulged residues demonstrated that deviations from the consensus sequence result in a decrease in the binding affinity of the RNA for the protein (Jaffrey *et al*., 1993). However, these studies did not rigorously define the structural and functional roles of each of the seven conserved residues. *In vitro* selection experiments were used to identify alternate RNA ligands for the iron regulatory protein. Initially, Henderson *et al*. (1996) discovered another IRE sequence that binds with high affinity to IRP1 but not IRP2; this IRP1-specific ligand contained the loop sequence 5′-UAGUAX-3′ where X was a U or C, but not a G or an A. In this sequence the C at position 1 is changed to a U and the only other change in the sequence is a G to A mutation at position 5. This co-variation led to the hypothesis that residues C_1 and G_5 in the loop form a base-pair in the wild-type sequence which could be an important structural feature of functional IREs (Henderson *et al*., 1994). By selecting for ligands against two different IRPs, Butt *et al*. (1996) noted that the RNA hairpins selected in a competitive binding study by IRP1 and IRP2 always contained a C at the bulge position, a G at position 3 of the loop and almost always contained an A at position 2 of the loop. Many of the selected sequences also had changes at position 4 of the loop, where the conserved U was either an A or a G, implying that sequence variation at this position did not significantly interfere with high-affinity binding. One of the goals of the present study is to complement the mutagenesis and biochemical studies with direct information on the conformation of the IRE RNA.

During the past decade, NMR spectroscopy has developed into an important tool for studying the three-dimensional structure of RNA in solution (for reviews see Varani & Tinoco, 1991; Pardi, 1995). NMR also represents an important probe of the dynamics of molecules in solution; for example NMR can be used to differentiate those parts of a molecule that are motionally disordered in solution from those that adopt a precise conformation. Here, we have applied heteronuclear multidimensional NMR techniques to study the structure and dynamics of the IRE RNA to help understand the structural basis for the consensus sequence of the RNA and how the RNA binds to the IRP1.

Results

Sequence design of the IREs used in the structural study

The sequence and secondary structure of the IRE found in the 5′ untranslated region of the human ferritin H-chain mRNA is shown in Figure 1(a) (Klausner *et al*., 1993). Residues 5 through 25 in the wild-type IRE sequence (Figure 1(b)) being studied here, are identical to residues 9 through 29 in the human ferritin H-chain IRE. The bottom four base-pairs in the lower stem were chosen to help improve the transcriptional efficiency with T7 RNA polymerase. Though formation of these four base-pairs is required to conform to the IRE consensus sequence, there is no sequence-specific requirement for these base-pairs (Bettany *et al*., 1992). Thus changes in the sequence of these base pairs have little or no effect on the binding of both IREs by human IRP1. The only difference between the wild-type and U_1A_5 IRE RNA hairpins shown in Figure 1 is in the hairpin loop where the wild-type has a 5′-CAGUGC-3′ loop sequence, whereas the U_1A_5 mutant IRE contains substitutions of U for C at residue 13 and A for G at residue 17

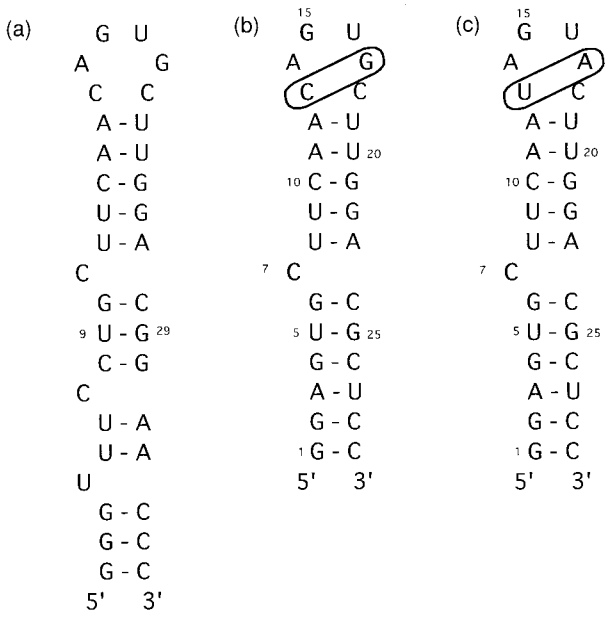

Figure 1. Nucleotide sequence and secondary structure of (a) the human ferritin H-chain IRE, (b) wild-type and (c) U_1A_5 mutant iron responsive element (IRE) RNAs. Residues 13 and 17, enclosed in ovals, form a base-pair in the NMR structures (see the text). The binding constants of these sequences for the human IRP1 are in the range of 20 to 40 pM (see the text)

(Figure 1(c)). Competition assays were used to measure the binding affinity of the IREs, depicted in Figure 1(b) and 1(c), for human IRP1, as described (Haile *et al.*, 1989; Jaffrey *et al.*, 1993). Based on measured IC_{50} values, the K_d values for binding of these RNAs to human IRP1 are 20 to 40 pM, which is not significantly different from the K_d for binding of the human ferritin H-chain IRE to human IRP1. Thus the sequences used here represent a biologically relevant form of the IRE RNA.

Assignments of exchangeable proton resonances

The one-dimensional (1D) proton NMR spectrum in H_2O of the wild-type IRE RNA is shown in Figure 2(a). The assignments were made on the basis of sequential NOE connectivities as described below. All of the imino proton resonances predicted by the secondary structure of the IRE RNA are observed in the 1D spectrum except for $U_{19}H3$ which only appears as a broad peak at 14.5 ppm in the spectrum collected at pH 5.5 (Figure 2(b)). Temperature studies of both the wild-type and the U_1A_5 IRE show that each RNA is stable because

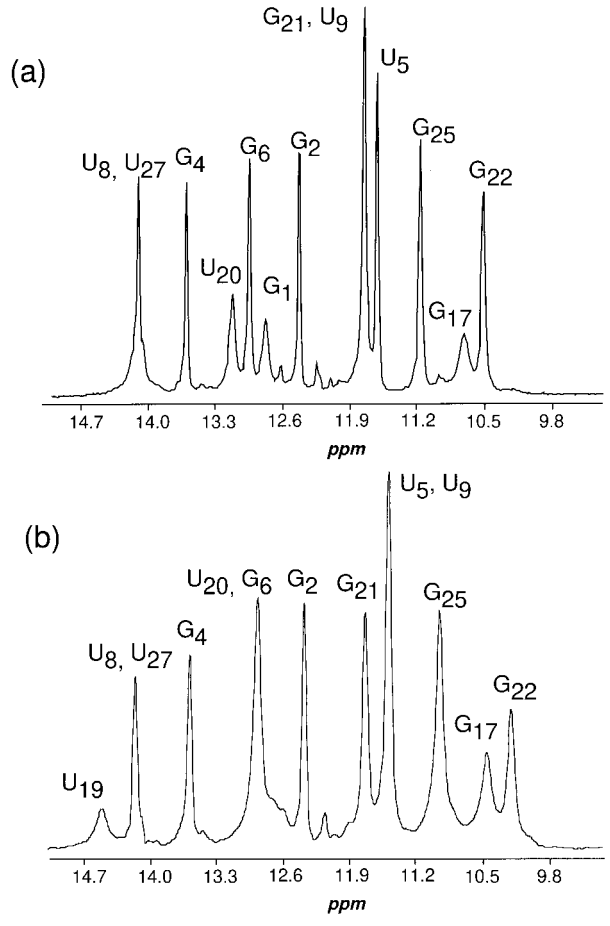

Figure 2. One-dimensional imino proton NMR spectra of the wild-type IRE RNA at (a) pH 6.5 and (b) at pH 5.5. The spectra were acquired at 10°C under conditions described in the text.

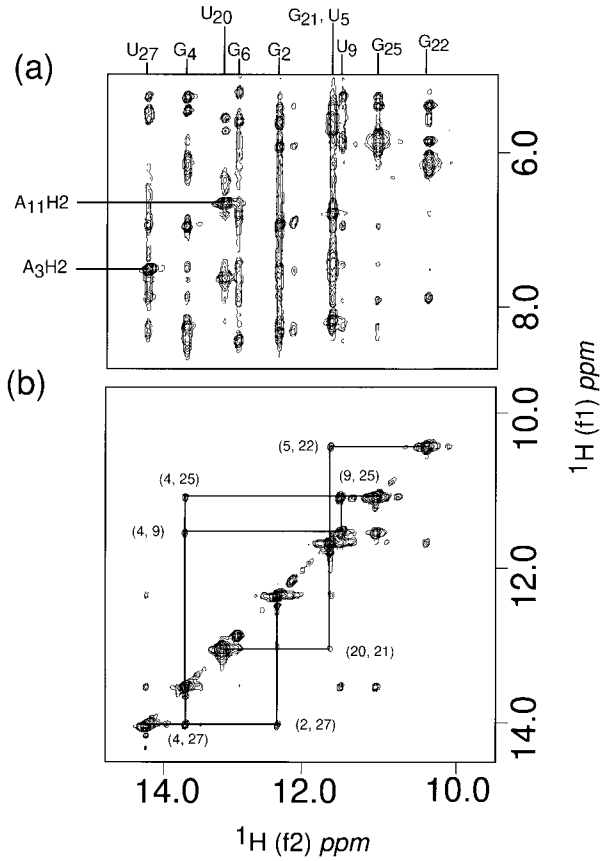

Figure 3. (a) Expanded region of the imino, amino and aromatic proton region of the H_2O NOESY spectrum of the wild-type IRE RNA at 10°C. Resonance assignment of the imino protons and the A_3H2 and $A_{11}H2$ are shown. (b) Imino proton to imino proton sequential NOE connectivities are illustrated. The spectrum was acquired with a sweep width of 12,000 Hz in both dimensions, 300 complex t_1 points of 80 scans and 2048 complex t_2 points.

imino proton resonances are observed up to 55°C (data not shown). A resonance at 10.7 ppm is observed in the imino proton spectrum of the wild-type IRE but not in the U_1A_5 IRE RNA (not shown). This resonance sharpens at pH 5.5 and was assigned as the imino proton of G_{17} in the loop, based on the guanine-specific ^{15}N chemical shift observed in the 2D (^{15}N,^{1}H) HSQC.

The exchangeable imino and amino protons of both the wild-type and U_1A_5 mutant IRE RNAs were assigned from (^{15}N,^{1}H) HSQC and NOESY spectra in H_2O at 15°C. The NOESY spectrum of the wild-type IRE is shown in Figure 3. The imino proton assignments were made from imino proton to imino proton sequential connectivities as illustrated in Figure 3. Sequential assignments of the lower helix were made starting with the $G_5 \cdot U_{25}$ wobble base-pair which has an extremely strong intra-base-pair NOE (Wüthrich, 1986). In the upper stem, only the imino proton to imino proton NOE cross-peak between G_{21} and U_{20} is observed; how-

Table 1. $^3J_{H1',H2'}$ coupling constants measured in the wild-type IRE RNA

Residue	G_1	G_2	A_3	G_4	U_5	G_6	C_7	U_8	U_9	C_{10}	A_{11}	A_{12}	C_{13}	A_{14}	G_{15}
$^3J_{H1',H2'}$ (Hz)	5.7	<2.0	<2.0	<2.0	<2.0	5.8	6.0	<2.0	N.O.	<2.0	N.O.	N.O.	<2.0	<2.0	11.6
Residue	U_{16}	G_{17}	C_{18}	U_{19}	U_{20}	G_{21}	G_{22}	A_{23}	C_{24}	G_{25}	C_{26}	U_{27}	C_{28}	C_{29}	
$^3J_{H1',H2'}$ (Hz)	10.5	5.7	5.6	<2.0	<2.0	<2.0	<2.0	<2.0	<2.0	<2.0	<2.0	<2.0	N.O.	N.O.	

N.O. indicates that these coupling constants could not be observed.

ever, sequential NOE connectivities between the $C_{10}\cdot G_{21}$ and the $U_9\cdot G_{22}$ base pairs were observed in a (^{15}N, ^{1}H) CPMG-NOESY spectrum (data not shown). The G_{17} imino proton showed a 1D NOE to a C amino proton at 8.25 ppm indicating that G_{17} forms a Watson-Crick base-pair with C_{13}. This base-pair has been observed in a previous NMR study of the upper stem and loop of the IRE (Laing & Hall, 1996).

Assignment of the non-exchangeable proton resonances

Recently developed triple resonance experiments that correlate exchangeable and non-exchangeable base protons in nucleic acids were next used to extend assignment of the exchangeable base protons to the H6 and H8 resonances for most of the residues in the upper and lower stems of the IRE (Simorre *et al*., 1996a,b, 1995). Pyrimidine H6 proton resonances were identified from the HNCCCH experiments and purine H8 resonances were identified from the HNC-TOCSY-CH experiments. The AH2 resonance assignments were also used to help identify the AH8 resonances. Two of these, A_3H2 and A_{11}H2, were identified by strong NOEs to the U_{27}H3 and U_{20}H3 protons, respectively, both of which are indicated in the H_2O NOESY shown in the top half of Figure 3. A_{23}H2 was identified from its NOE cross-peak to the U_8H3 in the H_2O NOESY spectrum at 1°C (data not shown). The A_{12}H2 and A_{14}H2 resonances were assigned from the (^{1}H,^{13}C) HSQC spectrum and from the 3D NOESY-HSQC spectrum.

Assignment of the ribose proton resonances began with H1′-C1′ correlations in a C2′ decoupled (^{1}H,^{13}C) HSQC spectrum. Once all 29 H1′-C1′ correlations were identified, the other ribose protons were assigned from a combination of (^{13}C,^{13}C,^{1}H) HCCH-TOCSY, 3D (^{1}H,^{13}C,^{1}H) HCCH-TOCSY and 3D (^{1}H,^{13}C,^{1}H) HCCH-COSY experiments (Pardi, 1995). Aromatic to H1′ and aromatic to H2′ sequential assignments were made from the 2D and 3D NOESY spectra using previously described methods (Nikonowicz & Pardi, 1993; Wüthrich, 1986). The intensity of the G_{15}H8-G_{15}H1′ cross-peak is much stronger than all the other aromatic to H1′ cross-peaks and comparable to the H5-H6 cross-peaks of U_5 and C_{26} (data not shown). In a short mixing time NOESY spectrum, the volume of this cross-peak integrates to a distance of approximately 2.5 Å and is twice the volume of the G_{15}H8 to H2′ cross-peak, indicating the glycosidic torsion angle for G_{15} is in the *syn* conformation.

Conformation of the sugars

The homonuclear three bond $^3J_{H1',H2'}$ coupling constants in Table 1 were measured directly from a 3D HCCH-E.COSY spectrum (Schwalbe *et al*., 1994). G_{15} and U_{16} have coupling constants greater than 10 Hz and therefore the ribose sugars of these two residues adopt primarily S-type puckers (Altona, 1982). G_1, G_6, C_7, G_{17} and C_{18} have values less than 10 Hz but greater than 2.0 Hz and are therefore interconverting between S-type and N-type sugar puckers. The ribose sugars of the other 22 residues have $^3J_{H1',H2'}$ coupling constants $\leqslant$2.0 Hz, which is characteristic of an N-type or C3′-*endo* conformation.

Structure calculations

A family of 15 refined, final structures of the IRE-1 were generated from 50 starting structures, as described in Materials and Methods. The three-dimensional structure of the RNA was calculated with 314 experimental NOE restraints, 153 torsion angle restraints and 54 base-pair constraints (see Table 2). No other restraints were included in the molecular dynamics calculations, and loose upper and lower bounds were applied to all NOE restraints to reflect the dynamic behavior of the RNA, as discussed below.

The relative orientation of the upper and lower stems is not well-defined because superposition of full structures led to an average pairwise RMSD of 4.0 Å; however, the local pairwise RMSDs reveal that the upper and lower stems form well-defined structural units. The average pairwise RMSDs for either the upper or lower stem increases when the

Table 2. Summary of NMR derived-distance and torsion angle restraints and root-mean-squared deviations for the final structures of the wild-type IRE RNA

NOE restraints	314
Interresidue	133
Intraresidue	181
Torsion angle restraints	153
Base-pairing restraints for upper and lower stems	54
	RMSD[a] (Å)
Lower stem (residues 1–6, 24–29)	1.71 ± 0.44
Lower stem and bulge (residues 1–7, 24–29)	2.14 ± 0.50
Upper stem (residues 8–12, 19–23)	1.63 ± 0.37
Upper stem and bulge (residues 7–12, 19–23)	2.19 ± 0.46
Loop residues 13, 14, 17	1.09 ± 0.29
Loop residues 13–18	2.44 ± 0.92

[a] These are the average pairwise RMSDs of the 15 refined structures.

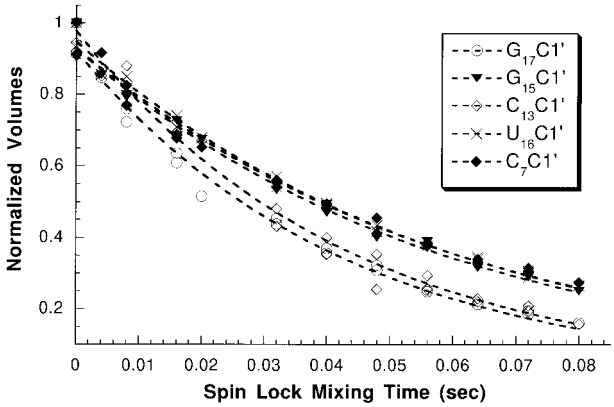

Figure 4. Plot of normalized volumes for H1′-C1′ cross-peaks *versus* ^{13}C spin lock mixing time for C_7, C_{13}, G_{15}, U_{16} and G_{17} in the $T_{1\rho}$ experiment. The non-linear least-squares fit of the data for each residue is shown with a broken line.

bulged C is included in the calculation (Table 2). This indicates that the conformation of the bulged C is not well defined. For the loop, the average pairwise RMSD for C_{13}, A_{14} and G_{17} is low but increases significantly when G_{15}, U_{16} and C_{18} are included in the calculation. This indicates that the conformation of loop residues C_{13}, A_{14} and G_{17} are well defined, whereas G_{15}, U_{16} and C_{18} are disordered in the structure.

Rotating spin-lattice relaxation times for C1′ sugar resonances

The rotating frame spin-lattice relaxation times, $T_1\rho$, were measured using a series of ^1H,^{13}C HSQC spectra with a ^{13}C spin lock (Yamazaki *et al.*, 1994). The ^1H-^{13}C correlations peaks decay exponentially as a function of ^{13}C spin lock mixing time. The $T_1\rho$ values for the C1′ resonances were calculated by a non-linear least-squares fit of this exponential decay, as illustrated in Figure 4. Because of resonance overlap, $T_1\rho$ values could not be calculated accurately for the A_{14} and C_{18} C1′ resonances. The C_7, G_{15} and U_{16} C1′ resonances have $T_1\rho$ values of 60 to 63 ms, which are significantly higher than the ~43 ms for the C_{13} and G_{17}C1′ resonances.

Discussion

Structure and dynamics of the IRE

A stereoview of one of the refined three-dimensional structures of the wild-type IRE is shown in Figure 5. The IRE forms a stem-loop structure that contains a single bulged C, where G_6 is base-paired to C_{24}, giving the secondary structure illustrated in Figure 1. The presence of this base-pair is consistent with recent *in vitro* selection studies that demonstrate that the human ferritin H-chain IRE requires that the nucleotide 5′ to the bulged C participates in a Watson-Crick base-pair (Butt *et al.*, 1996). An alternative representation of the secondary structure was previously proposed from computer modeling, where the bulge consists of three nucleotides having the sequence 5′-UGC-3′ instead of a single bulged C (Bettany *et al.*, 1992). However, both the NMR structure and the *in vitro* selection results rule out this alternate secondary structure for the IRE. The NMR data show that the IRE contains both well-defined and conformationally disordered regions. The upper and lower stems and residues C_{13}, A_{14} and G_{17} in the loop are well-defined whereas residues C_7 in the bulge, and

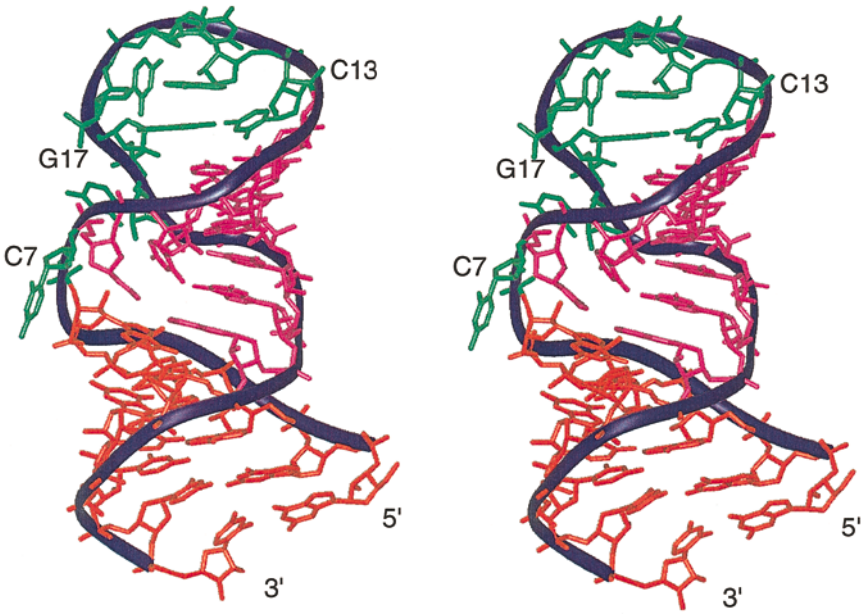

Figure 5. Stereoview of one of the 15 refined structures of the wild-type IRE RNA hairpin. The loop residues and the bulged C are shown in green, the lower stem is shown in orange, and the upper stem is shown in magenta.

G_{15}, U_{16} and C_{18} in the loop are not well-defined in the structure.

To investigate more thoroughly the motion of the residues in the bulge and loop regions of the IRE, the $T_1\rho$ relaxation times were measured in the wild-type IRE. The $T_1\rho$ relaxation times for the C1′ resonances on residues C_7, G_{15} and U_{16} are significantly longer than the $T_1\rho$ values for C1′ resonances on other residues (~60 *versus* ~43 ms). This indicates that the conformations of the bulged C_7 residue, and loop G_{15}, U_{16} residues are dynamic in the IRE, whereas the other loop residues have relaxation times similar to resonances in the stem regions. The difference in $T_1\rho$ values between flexible residues and well-defined residues correlates well with the local RMSDs reported in Table 2.

Structure and function of the lower and upper stems of the IRE-1

The refined average structures of both lower and upper stems are shown in Figures 6 and 7 and reveal that these regions of the IRE have an *A*-form conformation (Saenger, 1984). For the upper and lower stems, interresidue NOEs from the H2′ proton of residue n to the H6, H8 protons of residue $n+1$ are stronger than the intraresidue NOEs from pyrimidine H5 proton to H6 proton, characteristic of the *A*-form conformation. All the bases in the stem regions have *anti* glycosidic torsion angles and all the sugar puckers, with the exception of terminal G_1 and G_6, are N-type (near C3′-*endo*). These upper and lower stems are locally well defined but do not have a fixed orientation with respect to each other. This suggests that the junction between the two stems functions as a flexible hinge that could allow the RNA to undergo a global conformational change upon binding by the IRP. The U imino proton resonance of the $U_8 \cdot A_{23}$ base-pair is not observed in a 2D NOESY spectrum above 1°C; the intensity imino to imino NOE cross-peak of the $U_9 \cdot G_{22}$ base-pair in the upper stem is weaker than that of the $U_5 \cdot G_{25}$ base-pair in the lower stem. This suggests that the imino protons of the A·U and the G·U base-pairs above the bulged C have faster solvent exchange rates than the other internal base-pairs in the stem regions of the RNA. This supports the notion that the junction between the two stems is flexible.

The variation in length and lack of sequence specificity of the lower stem suggests that bases in the lower stem do not interact directly with the protein in the complex. However, *in vitro* selection experiments showed that formation of the $G_6 \cdot C_{24}$ base-pair adjacent to the bulged C in the lower stem favors high-affinity binding by the IRP1 and IRP2 (Butt *et al.*, 1996). Positioned between the bulge and the loop, the upper stem plays a more direct role in binding and regulation where a five-base-pair stem is required for iron-dependent regulation (Kikinis *et al.*, 1995). However, there is no sequence conservation for these base-pairs. This length requirement of the upper stem combined with the lack of sequence specificity for these base-pairs suggest that it functions primarily as a ''molecular ruler''. The upper stem would then provide the correct distance and spatial orientation between the bulged C_7 and G_{15} in the loop. In this model we propose that the bases of both C_7 and G_{15} make sequence-specific interactions with the IRP.

Conformation and function of the bulged C and hairpin loop

Figure 6 shows that the conformation of the bulged C_7 is not well-defined in the three-dimensional structures of wild-type IRE RNA. Deletion of this residue from RNA results in a ~400-fold decrease in the binding affinity as compared to the wild-type RNA (Jaffrey *et al.*, 1993). All RNAs in

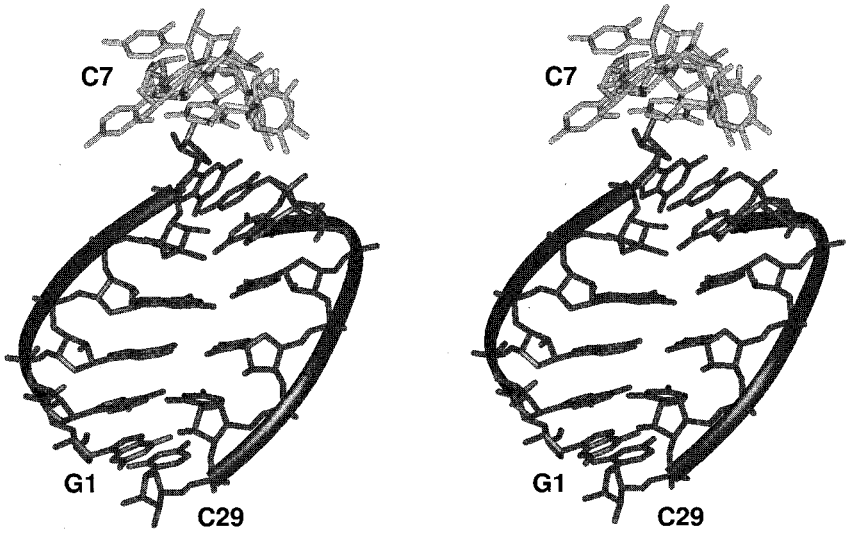

Figure 6. The relative positions of the bulged C_7 residue from the 15 low-energy structures of the wild-type IRE when superimposed on the average structure of the lower stem.

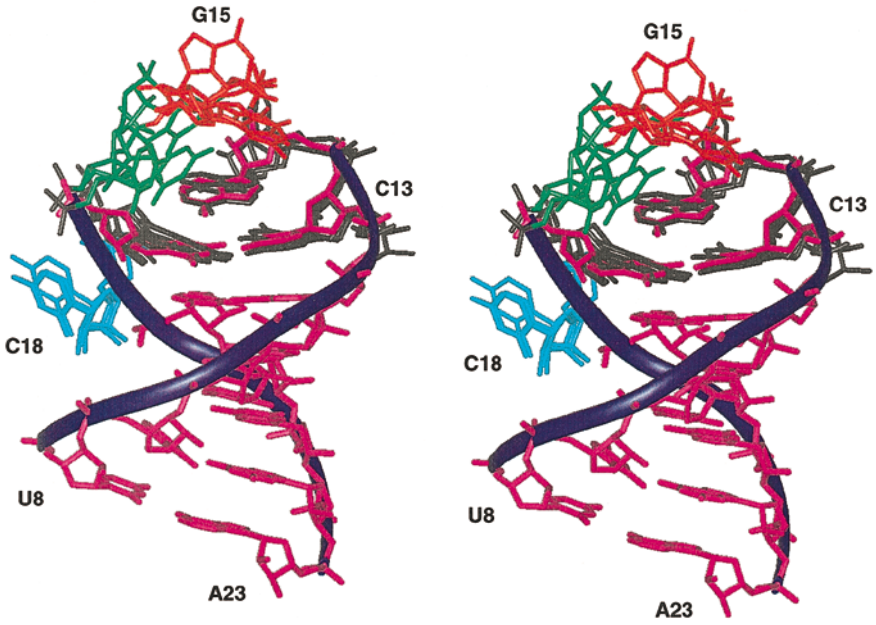

Figure 7. Stereoview illustrating the variation in the conformations of the loop residues of the refined structures of the wild-type IRE. The structures were superimposed on the average structure of the upper stem. Residues in the average structure are shown in magenta, residues C_{13}, A_{14} and G_{17} are in black, G_{15} in orange, U_{16} in green and C_{18} in cyan.

the *in vitro* selection experiments with IRP1 and IRP2 contain a cytosine at the bulge position (Butt *et al.*, 1996). This strongly suggests that the bulged C interacts directly with the protein in a sequence-specific manner; for example, the bulged C may form a hydrogen bond with a side-chain residue in the protein.

A superposition of the loop residues from the family of final converged structures overlaid with the average structure of the upper stem is displayed in Figure 7. Three residues in the loop, C_{13}, A_{14} and G_{17}, have well-defined conformations whereas these for G_{15}, U_{16} and C_{18} are not well-defined. Of the three flexible residues in the loop, only G_{15} is required for high-affinity binding of the RNA by the protein. The intensity of the G_{15}H8 to G_{15}H1′ NOE cross-peak is much stronger than the other intraresidue H8, H6 to H1′ NOE cross-peaks in this RNA. Although different relaxation properties of G_{15} could contribute to the strong intensity of this H8 to H1′ NOE cross-peak, the intensity of this cross-peak is twice that of the G_{15}H8 to G_{15}H2′ NOE cross-peak. Furthermore, the sugar pucker of G_{15} is S-type (near C2′-*endo*). Taken together, the NMR results indicate that G_{15} adopts a *syn*-type glycosidic angle within the range of motion of this residue. This *syn* conformation for G_{15} might be required for sequence-specific recognition of the RNA by the protein.

In the solution structure, C_{13} and G_{17} are base paired to each other. A_{14}, the other nucleotide in the loop that is well-defined, stacks directly above G_{17} (Figure 8). In almost all cases, the A is required at this position for high-affinity binding to the protein. A single point mutation of an A to a G in the IRE of the L-ferritin mRNA results in hyperferritinemia and bilateral cataract formation in humans (Beaumont *et al.*, 1995). The observation that the A to G mutation leads to development of a human disease clearly indicates that A_{14} is important for IRE function, though phylogenetic and biochemical evidence have not clearly defined its structural role. Similarly a mutation of G_{15} to C also results in severe cataract formation and hyperferritinemia in patients that carry this mutation (Girelli *et al.*, 1995). There are several indications that loop residues 1 (C_{13}) and 5 (G_{17}) do not interact directly with the protein but instead are important for the structure and stability of the loop. If C_{13} or G_{17} make base-specific contacts with the protein, it is unlikely that the U_1A_5 mutant IRE would have been selected as a high-affinity RNA ligand for the IRP1. UV melting studies of an IRE containing the

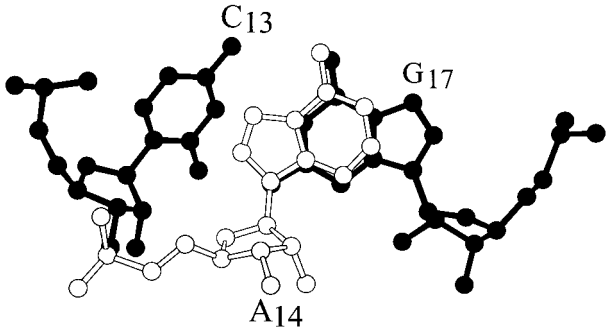

Figure 8. Conformation of C_{13}, A_{14} and G_{17} viewed down the helical axis, which shows how A_{14} stacks directly over G_{17}. This Figure was generated with MOLSCRIPT (Kraulis, 1991).

loop sequence 5′-CAGU**A**C-3′ lowers the T_m of the RNA (Laing & Hall, 1996; Sierzputowska-Gracz *et al*., 1995). This mutant is not bound by the IRP1 with high affinity (Jaffrey *et al*., 1993). This indicates that presence of this base-pair stabilizes the local conformation of the loop which is necessary for high-affinity binding and iron-dependent regulation. Formation of the $C_{13}\cdot G_{17}$ base-pair could explain why residue 18 cannot be a G. A G at position 18 would likely base-pair with C_{13} and therefore disrupt the base-pair between G_{17} and C_{13}. This would lead to a different conformation of the loop which could then result in loss of function.

Comparison with the U_1A_5 mutant

The loop regions of both wild-type and U_1A_5 mutant IRE RNAs are shown in Figure 9. Overall, the structural characteristics of the loop regions of these two IREs are nearly identical. Analogous to the wild-type sequence, the conformation of the bulged C in the U_1A_5 mutant IRE is not well defined. This suggests that the conformation of the bulged C is the same in a complex of either the wild-type or U_1A_5 mutant IRE with the IRP. For the loop region, G_{15}, U_{16} and C_{18} are not well-defined and have increased dynamics from C1′ $T_1\rho$ measurements, whereas U_{13}, A_{14} and A_{17} are well-defined. Identical with the wild-type sequence, G_{15} in the U_1A_5 RNA adopts a *syn* conformation.

In the NOESY spectrum of the U_1A_5 mutant IRE, A_{17}H2 has NOEs to A_{14}H1′ and to U_{19}H1′. This is consistent with a $U_{13}\cdot A_{17}$ base-pair in the loop, which is analogous to the $C_{13}\cdot G_{17}$ base pair of the wild-type IRE. However, no imino proton resonance was observed for U_{13}, therefore this imino proton is exchanging rapidly with solvent. Without direct evidence for base-pairing in the loop, two separate structure calculations were performed. In the first set, the base-pair between residue U_{13} and residue A_{17} was restrained. As expected, this base-pair was formed in all the final structures and these restraints did not introduce any significant distance violations. In the second set of calculations no restraints were included for this base-pair, and 30% of the final structures contained the base-pair whereas in the other structures the U_{13} and A_{17} were not well-defined. The $T_1\rho$ data are consistent with formation of the $U_{13}\cdot A_{17}$ base-pair and together these results indicate that a $U_{13}\cdot A_{17}$ base-pair occurs in the structure of the U_1A_5 mutant IRE, as suggested by the *in vitro* selection experiments (Henderson *et al*., 1994).

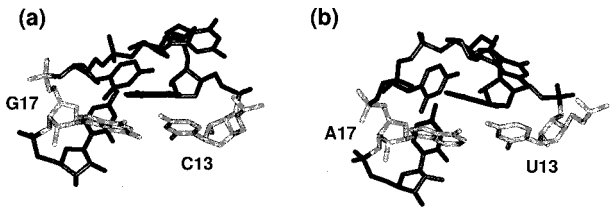

Figure 9. Structures of the loop region from (a) the wild-type IRE and (b) U_1A_5 IRE RNA hairpins. Residues 13 and 17 in the loop are shown in gray and form a Watson-Crick base pair in both of these sequences (see the text).

Comparison with other RNAs

The simultaneous presence of well-defined and flexible residues in the three-dimensional structure of the IRE has also been observed in the NMR structural studies of other RNAs, including the Rev response element (Battiste *et al*., 1995, 1994; Peterson *et al*., 1994), the 3′ untranslated region of the U1A pre-RNA (Allain *et al*., 1996), the TAR RNA (Puglisi *et al*., 1993), an ATP-binding aptamer RNA (Dieckmann *et al*., 1996; Jiang *et al*., 1996), and a theophylline-binding RNA aptamer (Zimmermann *et al*., 1997). For these RNAs, the residues critical to binding often appear disordered in the free RNA and become well-ordered upon complex formation. Thus we expect that the disordered residues C_7 and G_{15} in the IRE become well defined upon complex formation. However, we would not expect that the well-defined residues, C_{13}, A_{14} and G_{17}, will undergo a major conformational change upon complex formation.

Interaction of the IRE RNA with the IRP

The 4Fe-4S cluster form of IRP1 is a cytosolic aconitase (Kennedy *et al*., 1992), which catalyzes the isomerization of citrate to isocitrate, but cannot bind IREs with high affinity (Haile *et al*., 1989). Restoration of RNA-binding activity and destruction of aconitase activity occurs only when the 4Fe-4S cluster dissociates from the IRP1 in iron-depleted cells. The X-ray crystal structure of the pig heart mitochondrial aconitase has been solved (Robbins & Stout, 1989) and this protein has 30% sequence identity with human IRP1 (Rouault *et al*., 1991). The high sequence identity between IRP and mitochondrial aconitase suggests similar structures for both proteins. Unfortunately, there is no X-ray crystal structure of the apoprotein and it is not possible to dock the IRE RNA into the structure of the aconitase with the 4Fe-4S cluster in a way that is consistent with the NMR structure observed here and the mutagenesis data on the IRP1. Nevertheless, the NMR data combined with the biochemical results provide insights into how the IRP could interact with the IRE. UV-cross-linking studies (Basilion *et al*., 1994; Swenson & Walden, 1994) demonstrated that the IRE hairpin interacts with residues 121 to 130 in human IRP1. In mitochondrial aconitase, four active site arginine residues are involved in substrate binding and specificity (Zheng *et al*., 1992; Lauble *et al*., 1992). All four active site arginine residues are found in IRP1, and site-directed mutagenesis reveals that three of these arginine residues are important in IRE binding (Butt *et al*., 1996; Philpott *et al*., 1993). In IRP1, mutagenesis of arginine 541 or 780 to glutamine (residues 452 and 644 in pig heart mito-

chondrial aconitase) results in a 10^3 to 10^4-fold decrease in binding affinity (Philpott *et al*., 1994). Arginine to guanine hydrogen bonds have been observed in the three-dimensional structure of several protein-DNA complexes, including zif268 (Pavletich & Pabo, 1991), the glucocorticoid receptor (Luisi *et al*., 1991), and *Escherichia coli* Trp repressor (Otwinowski *et al*., 1988), and it is possible that G_{15} in the IRE forms a specific interaction with an active site arginine in the IRP. When the 4Fe-4S cluster is bound to the protein, the binding cleft, situated between domains 1 to 3 and domain 4, is in a ''closed'' state, which permits arginine 541 or 780 to bind isocitrate (Lauble *et al*., 1992) but prevents these amino acid residues from interaction with residues in the hairpin loop of the IRE. This may be one way the presence of the 4Fe-4S cluster inhibits high affinity binding of the RNA. It is likely that these arginine residues become accessible to the RNA when the cleft is opened up by a conformational change in the hinge linker peptide that connects domain 3 and domain 4 (Lauble *et al*., 1992; Basilion *et al*., 1994). Recently, Schalinske *et al.* (1997) demonstrated an increase in the rate of proteolysis of sites near the proposed binding cleft and hinge linker regions of the protein when the 4Fe-4S cluster was removed. This indicates that the cleft cannot exist in this ''open'' state without dissociation of the 4Fe-4S cluster.

The crystal structure of a complex of the coat protein from MS2 bacteriophage with its operator RNA has been determined (Valegard *et al*., 1994) and the RNA has a hairpin-single base bulge motif that has a qualitatively similar structure to the IRE RNA (Borer *et al*., 1995). For the MS2 complex, the loop and bulged residues of the operator RNA that are essential for binding form hydrogen bond and/or stacking interactions with conserved amino acid residues (Valegard *et al*., 1994). In addition, the protein makes specific contacts with the phosphate backbone of the RNA. We expect that similar types of interactions will be observed in the IRP1-IRE complex. We are currently testing this hypothesis by photo-cross-linking studies of the protein-RNA complex and modifications of the critical nucleotides in the IRE RNA hairpin.

Materials and Methods

Sample preparation

The wild-type and U_1A_5 IRE RNAs shown in Figure 1 were synthesized by *in vitro* transcription on a single-stranded DNA template using phage T7 RNA polymerase. The transcription reactions were performed using standard conditions except each reaction contained a total NTP concentration of 8 mM (Milligan *et al*., 1987). The $^{13}C/^{15}N$ NTPs were prepared as described (Nikonowicz *et al*., 1992; Batey *et al*., 1992). The crude RNA from each transcription reaction was purified by preparative gel electrophoresis with a 20% (w/v) denaturing gel containing 7 M urea. For each gel, the product band was visualized with UV shadowing and then excised from the gel. The RNA was recovered from the excised product band by electroelution and ethanol precipitation of the electroeluant. The RNA was further purified by ion-exchange DEAE Sephacel chromatography. Fractions from the ion-exchange column containing the RNA were then dialyzed extensively against an NMR buffer solution of 10 mM sodium phosphate (pH 6.5), 10 mM NaCl, 0.2 mM EDTA. A 5 mg sample of purified $^{13}C/^{15}N$-labeled wild-type IRE was synthesized from a 50 ml transcription which yielded a 1.5 mM sample in 350 µl. A 4.5 mg sample of the purified, uniformly $^{13}C/^{15}N$-labeled, mutant U_1A_5 IRE was obtained from a 40 ml transcription reaction yielding a 1.2 mM sample in 350 µl. Before acquisition of NMR data, the samples were heated to 85°C for two minutes and then snap-cooled on ice to induce formation of the RNA hairpin.

NMR Spectroscopy

All NMR experiments were performed at 500 MHz on either Varian VXR or UnityPlus instruments equipped with pulsed-field gradients. All spectra were transformed with the program FELIX version 2.30 or 95.0 (Biosym/ MSI, San Diego, CA). A variety of homo- and heteronuclear magnetic resonance experiments were used to make resonance assignments and to generate structural constraints for the IRE RNAs including: 2D ($^1H,^1H$) NOESY (Kumar *et al*., 1980) and ($^1H,^1H$) DQF-COSY (Rance *et al*., 1983); 2D ($^{15}N,^1H$) HSQC, 2D ($^{13}C,^1H$) HSQC, 2D ($^{15}N,^1H$) HNCCCH (Simorre *et al*., 1995), 2D ($^{15}N,^1H$) HNC-TOCSY-CH (Simorre *et al*., 1996a,b), 2D ($^{15}N,^1H$) CPMG-NOESY (Mueller *et al*., 1995), 3D ($^1H,^{13}C,^1H$) HCCH-E.COSY (Schwalbe *et al*., 1994), 3D ($^{13}C,^{13}C,^1H$) HCCH-TOCSY, 3D ($^1H,^{13}C,^1H$) HCCH-TOCSY, 3D ($^1H,^{13}C,^1H$) HCCH-COSY, and 3D ($^1H,^{13}C,^1H$) NOESY-HSQC (Pardi, 1995) experiments. For all two-dimensional and three-dimensional heteronuclear experiments, ^{13}C or ^{15}N WALTZ or GARP broadband decoupling was applied during the acquisition period. A DIPSI-2 mixing scheme was applied during the 25 ms ^{13}C spin lock period in the HCCH-TOCSY experiments. In the NOESY and HSQC spectra acquired in 90% H_2O/ 10% ^2H_2O, water suppression was performed with either 11 echo (Sklenár & Bax, 1987) or flip-back WATERGATE pulses (Piotto *et al*., 1992).

Structure determination

For each RNA molecule, interproton distance restraints were obtained from three 3D ($^1H,^{13}C,^1H$) NOESY-HSQC spectra at mixing times of 75, 180 and 300 ms. NOE cross-peak intensities were classified as strong if their intensities were greater than or equal to those of the pyrimidine H5 to H6 cross-peaks in the 75 ms 3D NOESY spectrum, medium if they were observed in the 75 ms and the 180 ms mixing time 3D NOESY spectra and their intensities were weaker than the pyrimidine H5 to H6 cross-peak, and weak if they were observed only in the 300 ms mixing time 3D NOESY spectrum. The lower distance bounds for all interproton distance pairs were set to 1.8 Å. Upper distance bounds of 3.5, 4.5 and 5.5 Å were applied for strong, medium and weak NOE cross-peaks, respectively. An additional upper bound of 1.0 Å was applied to NOE cross-peaks involving exchangeable protons in the NOESY spectrum in H_2O at 10°C. Hydrogen-bonding constraints were included for the 11 base-pairs of the upper and lower stems, as described (Jucker *et al*., 1996). Sugar pucker conformations were classified as N-type (near C3′-*endo*), S-type (near C2′-*endo*) or mixed confor-

mation based on the $J_{H1',H2'}$ coupling constants (Altona, 1982) measured in a 3D (^1H,^{13}C,^1H) HCCH-E.COSY spectrum. For sugars falling into either N-type or S-type conformations the ν_0 to ν_4 endocyclic torsion angles were restrained to published values and no restraints were included for sugars showing mixed conformation (Saenger, 1984). For residues with resolved H2′-C2′ correlation peaks in a spin echo difference CT-HSQC spectrum, the ε torsion angles were calculated from measured $^3J_{C2'P}$ coupling constants (Legault *et al*., 1995). Most of these coupling constants were obtained for residues in the loop and the bulge.

All calculations were performed on a Silicon Graphics Indigo^2 workstation using X-PLOR version 3.1 (Brünger, 1992). A total of 50 initial structures were generated by randomizing the backbone torsion angles of the linearized 29mer RNA molecule. Refinement of these starting structures occurred in three stages. In the first stage, the molecules were subjected to a simulated annealing protocol, where each structure was heated to 3000 K and then cooled to 300 K over 15 ps of restrained molecular dynamics. This allowed the RNA to fold into its global hairpin conformation. During this stage, only experimental distance and hydrogen bonding restraints were used. In the second stage, experimental dihedral angle restraints were included in the refinement procedure, which consisted of 2.5 ps of simulated annealing at 3000 K after which the bath was cooled to 300 K over 6.25 ps. In the final step, the refined structures underwent 1000 steps of restrained energy minimization. Of the 50 starting structures, the 15 lowest energy structures that had no violations greater than 0.3 Å were selected for analysis and all these structures had a total potential energy of less than −100 kcal/mol. Coordinates of the final structures have been deposited in the Protein Data Bank under accession number 1AQO.

Acknowledgments

This work was supported in part by NIH grant AI33098 to A. P. and NIH NRSA Fellowship GM16577 to K. J. A. We thank the Colorado RNA Center for their support of RNA science on the Boulder campus.

References

Allain, F. H., Gubser, C. C., Howe, P. W., Nagai, K., Neuhaus, D. & Varani, G. (1996). Specificity of ribonucleoprotein interaction determined by RNA folding during complex formulation. *Nature,* **380**, 646–650.

Altona, C. (1982). Conformational analysis of nucleic acids. Determination of backbone geometry of single-helical RNA and DNA in aqueous solution. *Rec. Trav. Chim. Pays-Bas.* **101**, 413–432.

Aziz, N. & Munro, H. N. (1987). Iron regulates ferritin mRNA translation through a segment of its 5′ untranslated region. *Proc. Natl Acad. Sci. USA,* **84**, 8478–82.

Barton, H. A., Eisenstein, R. S., Bomford, A. & Munro, H. N. (1990). Determinants of the interaction between the iron-responsive element-binding protein and its binding site in rat L-ferritin mRNA. *J. Biol. Chem.* **265**, 7000–7008.

Basilion, J. P., Rouault, T. A., Massinople, C. M., Klausner, R. D. & Burgess, W. H. (1994). The iron-responsive element-binding protein: localization of the RNA-binding site to the aconitase active-site cleft. *Proc. Natl Acad. Sci. USA,* **91**, 574–8.

Batey, R. T., Inada, M., Kujawinski, E., Puglisi, J. D. & Williamson, J. R. (1992). Preparation of isotopically labeled ribonucleotides for multidimensional NMR spectroscopy of RNA. *Nucl. Acids Res.* **20**, 4515–4523.

Battiste, J. L., Tan, R., Frankel, A. D. & Williamson, J. R. (1994). Binding of an HIV Rev peptide to Rev responsive element RNA induces formation of purine-purine base pairs. *Biochemistry,* **33**, 2741–2747.

Battiste, J. L., Tan, R., Frankel, A. D. & Williamson, J. R. (1995). Assignment and modeling of the Rev response element RNA bound to a Rev peptide using ^{13}C-heteronuclear NMR. *J. Biomol. NMR,* **6**, 375–389.

Beaumont, C., Leneuve, P., Devaux, I., Scoazec, J. Y., Berthier, M., Loiseau, M. N., Grandchamp, B. & Bonneau, D. (1995). Mutation in the iron responsive element of the L ferritin mRNA in a family with dominant hyperferritinaemia and cataract. *Nature Genet.* **11**, 444–446.

Bettany, A. J., Eisenstein, R. S. & Munro, H. N. (1992). Mutagenesis of the iron-regulatory element further defines a role for RNA secondary structure in the regulation of ferritin and transferrin receptor expression. *J. Biol. Chem.* **267**, 16531–16537.

Binder, R., Horowitz, J. A., Basilion, J. P., Koeller, D. M., Klausner, R. D. & Harford, J. B. (1994). Evidence that the pathway of transferrin receptor messenger-RNA degradation involves an endonucleolytic cleavage within the 3′ UTR and does not involve poly(A) tail shortening. *EMBO J.* **13**, 1969–1980.

Borer, P. N., Lin, Y., Wang, S., Roggenbuck, M. W., Gott, J. M., Uhlenbeck, O. C. & Pelczer, I. (1995). Proton NMR and structural features of a 24–nucleotide RNA hairpin. *Biochemistry*, **34**, 6488–6503.

Brünger, A. T. (1992). *X-PLOR, Version 3.1: A System for X-ray Crystallography and NMR,* Yale University Press, New Haven, CT.

Butt, J., Kim, H. Y., Basilion, J. P., Cohen, S., Iwai, K., Philpott, C. C., Altschul, S., Klausner, R. D. & Rouault, T. A. (1996). Differences in the RNA binding sites of iron regulatory proteins and potential target diversity. *Proc. Natl Acad. Sci. USA,* **93**, 4345–4349.

Dieckmann, T., Suzuki, E., Nakamura, G. K. & Feigon, J. (1996). Solution structure of an ATP-binding RNA aptamer reveals a novel fold. *RNA,* **2**, 628–640.

Girelli, D., Corrocher, R., Bisceglia, L., Olivieri, O., Defranceschi, L., Zelante, L. & Gasparini, P. (1995). Molecular-basis for the recently described hereditary hyperferritinemia cataract syndrome: a mutation in the iron-responsive element of ferritin L-subunit gene (the Verona Mutation). *Blood,* **86**, 4050–4053.

Gray, N. K. & Hentze, M. W. (1994). Iron regulatory protein prevents binding of the 43 S translation preinitiation complex to ferritin and eALAS messenger-RNAs. *EMBO J.* **13**, 3882–3891.

Guo, B., Yu, Y. & Leibold, E. A. (1994). Iron regulates cytoplasmic levels of a novel iron-responsive element-binding protein without aconitase activity. *J. Biol. Chem.* **269**, 24252–24260.

Haile, D. J., Hentze, M. W., Rouault, T. A., Harford, J. B. & Klausner, R. D. (1989). Regulation of interaction of the iron-responsive element binding pro-

tein with iron-responsive RNA elements. *Mol. Cell. Biol.* **9**, 5055–5061.

Harrell, C. M., McKenzie, A. R., Patino, M. M., Walden, W. E. & Theil, E. C. (1991). Ferritin mRNA: interactions of iron regulatory element with translational regulator protein P-90 and the effect on base-paired flanking regions. *Proc. Natl Acad. Sci. USA,* **88**, 4166–4170.

Henderson, B. R., Menotti, E., Bonnard, C. & Kuhn, L. C. (1994). Optimal sequence and structure of iron-responsive elements. Selection of RNA stem-loops with high affinity for iron regulatory factor. *J. Biol. Chem.* **269**, 17481–17489.

Henderson, B. R., Menotti, E. & Kuhn, L. C. (1996). Iron regulatory proteins 1 and 2 bind distinct sets of RNA target sequences. *J. Biol. Chem.* **271**, 4900–4908.

Hentze, M. W. & Kuhn, L. C. (1996). Molecular control of vertebrate iron metabolism: mRNA-based regulatory circuits operated by iron, nitric oxide, and oxidative stress. *Proc. Natl Acad. Sci. USA,* **93**, 8175–8182.

Hentze, M. W., Caughman, S. W., Rouault, T. A., Barriocanal, J. G., Dancis, A., Harford, J. B. & Klausner, R. D. (1987). Identification of the iron-responsive element for the translational regulation of human ferritin mRNA. *Science,* **238**, 1570–1573.

Jaffrey, S. R., Haile, D. J., Klausner, R. D. & Harford, J. B. (1993). The interaction between the iron-responsive element binding protein and its cognate RNA is highly dependent upon both RNA sequence and structure. *Nucl. Acids Res.* **21**, 4627–4631.

Jiang, F., Kumar, R. A., Jones, R. A. & Patel, D. J. (1996). Structural basis of RNA folding and recognition in an AMP-RNA aptamer complex. *Nature,* **382**, 183–186.

Jucker, F. M., Heus, H. A., Yip, P. F., Moors, E. H. M. & Pardi, A. (1996). A network of heterogeneous hydrogen bonds in GNRA tetraloops. *J. Mol. Biol.* **264**, 968–980.

Kennedy, M. C., Mendemueller, L., Blondin, G. A. & Beinert, H. (1992). Purification and characterization of cytosolic aconitase from beef-liver and its relationship to the iron-responsive element binding-protein. *Proc. Natl Acad. Sci. USA,* **89**, 11730–11734.

Kikinis, Z., Eisenstein, R. S., Bettany, A. J. & Munro, H. N. (1995). Role of RNA secondary structure of the iron-responsive element in translational regulation of ferritin synthesis. *Nucl. Acids Res.* **23**, 4190–4195.

Klausner, R. D., Rouault, T. A. & Harford, J. B. (1993). Regulating the fate of mRNA: the control of cellular iron metabolism. *Cell,* **72**, 19–28.

Kraulis, P. J. (1991). MOLSCRIPT: a program to produce both detailed and schematic plots of protein structures. *J. Appl. Crystallog.* **24**, 946–950.

Kumar, A., Ernst, R. R. & Wüthrich, K. (1980). A two-dimensional nuclear Overhauser enhancement (2D NOE) experiment for the elucidation of complete proton-proton cross-relaxation networks in biological macromolecules. *Biochem. Biophys. Res. Commun.* **95**, 1–6.

Laing, L. G. & Hall, K. B. (1996). A model of the iron responsive element RNA hairpin loop structure determined from NMR and thermodynamic data. *Biochemistry,* **35**, 13586–13596.

Lauble, H., Kennedy, M. C., Beinert, H. & Stout, C. D. (1992). Crystal-structures of aconitase with isocitrate and nitroisocitrate bound. *Biochemistry,* **31**, 2735–2748.

Legault, P., Jucker, F. M. & Pardi, A. (1995). Improved measurement of ^{13}C-^{31}P coupling constants in isotopically labeled RNA. *FEBS Letters,* **362**, 156–160.

Luisi, B. F., Xu, W. X., Otwinowski, Z., Freedman, L. P., Yamamoto, K. R. & Sigler, P. B. (1991). Crystallographic analysis of the interaction of the glucocorticoid receptor with DNA. *Nature,* **352**, 497–505.

Milligan, J. F., Groebe, D. R., Witherell, G. W. & Uhlenbeck, O. C. (1987). Oligoribonucleotide synthesis using T7 RNA polymerase and synthetic DNA templates. *Nucl. Acids Res.* **15**, 8783–8789.

Mueller, L., Legault, P. & Pardi, A. (1995). Improved RNA structure determination by detection of NOE contacts to exchange-broadened amino protons. *J. Am. Chem. Soc.* **117**, 11043–11048.

Nikonowicz, E. P. & Pardi, A. (1993). An efficient procedure for assignment of the proton, carbon and nitrogen resonances in $^{13}C/^{15}N$ labeled nucleic acids. *J. Mol. Biol.* **232**, 1141–1156.

Nikonowicz, E. P., Sirr, A., Legault, P., Jucker, F. M., Baer, L. M. & Pardi, A. (1992). Preparation of ^{13}C and ^{15}N labelled RNAs for heteronuclear multidimensional NMR studies. *Nucl. Acids Res.* **20**, 4507–4513.

Otwinowski, Z., Schevitz, R. W., Zhang, R. G., Lawson, C. L., Joachimiak, A., Marmorstein, R. Q., Luisi, B. F. & Sigler, P. B. (1988). Crystal structure of trp repressor/operator complex at atomic resolution. *Nature,* **335**, 321–329.

Pardi, A. (1995). Multidimensional heteronuclear NMR experiments for structure determination of isotopically labeled RNA. *Methods Enzymol.* **261**, 350–380.

Pavletich, N. P. & Pabo, C. O. (1991). Zinc finger-DNA recognition: crystal structure of a Zif268-DNA complex at 2.1 Å. *Science,* **252**, 809–817.

Peterson, R. D., Bartel, D. P., Szostak, J. W., Horvath, S. J. & Feigon, J. (1994). ^{1}H-NMR studies of the high-affinity rev binding-site of the rev responsive element of HIV-1 messenger-RNA: base pairing in the core binding-element. *Biochemistry,* **33** (18), 5357–5366.

Philpott, C. C., Haile, D., Rouault, T. A. & Klausner, R. D. (1993). Modification of a free Fe-S cluster cysteine residue in the active iron-responsive element-binding protein prevents RNA binding. *J. Biol. Chem.* **268**, 17655–17658.

Philpott, C. C., Klausner, R. D. & Rouault, T. A. (1994). The bifunctional iron-responsive element binding protein/cytosolic aconitase: the role of active-site residues in ligand binding and regulation. *Proc. Natl Acad. Sci. USA,* **91**, 7321–7325.

Piotto, M., Saudek, V. & Sklenar, V. (1992). Gradient-tailored excitation for single-quantum NMR-spectroscopy of aqueous-solutions. *J. Biomol. NMR,* **2**, 661–665.

Puglisi, J. D., Chen, L., Frankel, A. D. & Williamson, J. R. (1993). Role of RNA structure in arginine recognition of TAR RNA. *Proc. Natl Acad. Sci. USA,* **90**, 3680–3684.

Rance, M., Sørensen, O. W., Bodenhausen, G., Wagner, G., Ernst, R. R. & Wüthrich, K. (1983). Improved spectral resolution in COSY ^{1}H NMR spectra of proteins via double quantum filtering. *Biochem. Biophys. Res. Commun.* **117**, 479–485.

Robbins, A. H. & Stout, C. D. (1989). Structure of activated aconitase: formation of the [4Fe-4S] cluster in

the crystal. *Proc. Natl Acad. Sci. USA,* **86**, 3639–3643.
Rouault, T. A., Stout, C. D., Kaptain, S., Harford, J. B. & Klausner, R. D. (1991). Structural relationship between an iron-regulated RNA-binding protein (IRE-BP) and aconitase: functional implications. *Cell,* **64**, 881–883.
Rouault, T. A., Haile, D. J., Downey, W. E., Philpott, C. C., Tang, C., Samaniego, F., Chin, J., Paul, I., Orloff, D. & Harford, J. B., *et al.* (1992). An iron-sulfur cluster plays a novel regulatory role in the iron-responsive element binding protein. *Biometals,* **5**(3), 131–140.
Saenger, W. (1984). *Principles of Nucleic Acid Structure,* Springer-Verlag, New York.
Samaniego, F., Chin, J., Iwai, K., Rouault, T. A. & Klausner, R. D. (1994). Molecular characterization of a second iron-responsive element binding protein, iron regulatory protein 2. Structure, function, and post-translational regulation. *J. Biol. Chem.* **269**, 30904–30910.
Schalinkse, K. L., Anderson, S. L., Tuazon, P. T., Chen, O. S., Kennedy, M. C. & Eisenstein, R. S. (1997). The iron-sulfur cluster of iron regulatory protein 1 modulates the accessibility of RNA binding and phosphorylation sites. *Biochemistry,* **36**, 3950–3958.
Schwalbe, H., Marino, J. P., King, G. C., Wechselberger, R., Bermel, W. & Griesinger, C. (1994). Determination of a complete set of coupling-constants in ^{13}C-labeled oligonucleotides. *J. Biomol. NMR,* **4**, 631–644.
Sierzputowska-Gracz, H., McKenzie, R. A. & Theil, E. C. (1995). The importance of a single G in the hairpin loop of the iron responsive element (IRE) in ferritin mRNA for structure: an NMR spectroscopy study. *Nucl. Acids Res.* **23**, 146–153.
Simorre, J.-P., Zimmermann, G. R., Pardi, A., Farmer, B. T. I. I. & Mueller, L. (1995). Triple resonance HNNCCH experiments for correlating exchangeable and nonexchangeable cytidine and uridine base protons in RNA. *J. Biomol. NMR,* **6**, 427–432.
Simorre, J.-P., Zimmermann, G. R., Mueller, L. & Pardi, A. (1996a). Triple-resonance experiments for assignment of adenine base resonances in ^{13}C/^{15}N-labeled RNA. *J. Am. Chem. Soc.* **118**, 5316–5317.
Simorre, J.-P., Zimmermann, G. R., Mueller, L. & Pardi, A. (1996b). Correlation of the guanosine exchangeable and nonexchangeable base protons in ^{13}C-/^{15}N-labeled RNA with an HNC-TOCSY-CH experiment. *J. Biomol. NMR,* **7**, 153–156.
Sklenár, V. & Bax, A. (1987). Spin-echo water suppression for the generation of pure-phase two-dimensional NMR spectra. *J. Magn. Reson.* **74**, 469–479.
Swenson, G. R. & Walden, W. E. (1994). Localization of an RNA-binding element of the iron-responsive element-binding protein within a proteolytic fragment containing iron coordination ligands. *Nucl. Acids Res.* **22**, 2627–2633.
Theil, E. C. (1994). Iron regulatory elements (IREs): a family of mRNA non-coding sequences. *Biochem. J.* **304**, 1–11.
Varani & Tinoco (1991). RNA structure and NMR spectroscopy. *Quart. Rev. Biophys.* **24**, 479–532.
Valegard, K., Murray, J. B., Stockley, P. G., Stonehouse, N. J. & Liljas, L. (1994). Crystal structure of a bacteriophage-RNA coat protein-operator complex. *Nature,* **371**, 623–626.
Wang, Y. H., Sczekan, S. R. & Theil, E. C. (1990). Structure of the 5′ untranslated regulatory region of ferritin mRNA studied in solution. *Nucl. Acids Res.* **18**, 4463–8.
Wang, Y. H., Lin, P. N., Sczekan, S. R., McKenzie, R. A. & Theil, E. C. (1991). Ferritin mRNA probed, near the iron regulatory region, with protein and chemical (1,10-phenanthroline-Cu) nucleases. A possible role for base-paired flanking regions. *Biol. Met.* **4**, 56–61.
Wüthrich, K. (1986). *NMR of Proteins and Nucleic Acids,* John Wiley & Sons, New York.
Yamazaki, T., Muhandiram, R. & Kay, L. E. (1994). NMR experiments for the measurement of carbon relaxation properties in highly enriched, uniformly ^{13}C,^{15}N-labeled proteins: application to $^{13}C^{\alpha}$ carbons. *J. Am. Chem. Soc.* **116**, 8266–8278.
Zheng, L., Kennedy, M. C., Beinrt, H. & Zalkin, H. (1992). Mutational analysis of active-site residues in pig-heart aconitase. *J. Biol. Chem.* **267**, 7895–7903.
Zimmermann, G. R., Jenison, R. D., Wick, C. L., Simorre, J.-P. & Pardi, A. (1997). Interlocking structural motifs mediate molecular discrimination by a theophylline-binding RNA. *Nature-Struct. Biol.* **4**, 644–649.

Edited by I. Tinoco

(Received 12 June 1997; received in revised form 18 August 1997; accepted 18 August 1997)

http://www.hbuk.co.uk/jmb

Supplementary material for this paper comprising two Tables and one Figure is available from JMB Online.